

Optical frequency combs significantly spanned to broad bandwidths by an optomechanical resonance

Xin Gu,¹ Jinlian Zhang,¹ Shulin Ding,² Xiaoshun Jiang,² Bing He,^{3,*} and Qing Lin^{1,†}

¹*Fujian Key Laboratory of Light Propagation and Transformation & Institute of Systems Science, College of Information Science and Engineering, Huaqiao University, Xiamen 361021, China*

²*National Laboratory of Solid State Microstructures and College of*

Engineering and Applied Sciences, Nanjing University, Nanjing 210093, China

³*Multidisciplinary Center for Physics, Universidad Mayor, Camino La Pirámide 5750, Huechuraba, Chile*

Optical frequency comb, as a spectrum made of discrete and equally spaced spectral lines, is a light source with essential applications in modern technology. Cavity optomechanical systems were found to be a feasible candidate for realizing on-chip frequency comb with low repetition rate. However, it was difficult to increase the comb line numbers of this type of frequency combs because the mechanical oscillation amplitude of such system, which determines the frequency comb bandwidth, cannot quickly increase with pump laser power. Here, we develop a new approach to generate broadband optomechanical frequency comb by employing a different mechanism to enhance the mechanical oscillation. Two pump tones with their frequency difference matching the mechanical frequency will drive the system into a self-organized nonlinear resonance and thus tremendously transfer the energy to the mechanical resonator. As a result, more than 10000 or even more comb lines become available under the pump laser power in the order of milliwatt. A unique feature of the self-organized resonance is the mechanical frequency locking so that, within a certain range of the frequency difference between two drive tones, the distance between comb teeth can be locked by the two drive tones and becomes independent of any change of pump power. This property guarantees a stable repetition rate of the generated frequency comb.

I. INTRODUCTION

Optical frequency combs, a light source of a series of discrete and equally spaced frequencies, have found wide applications in modern technology, such as optical clock [1], astronomical spectrograph calibration [2], precision time/frequency transfer [3], ultraviolet and infrared (IR) spectroscopy [4–6], precision distance measurement [7], optical communication [8], and others. In the past, the main technologies developed to generate optical frequency combs are confined to mode-locked femtosecond lasers [9, 10], electro-optic modulation of a continuous-wave laser [11], and parametric frequency conversion through cascaded four-wave mixing [12–16]. Optomechanical nonlinearity in a micro-cavity [17–19], as well as the related magnonic realization [20], is a recently interested approach to realize such light source known as optomechanical-optical frequency comb (OMOFC). OMOFCs are repeated pulses at the corresponding mechanical frequencies, which are relatively low, e.g, less than 1 GHz, and such low-repeating OMOFCs are highly relevant to some states-of-art technologies like high-resolution spectroscopy [21, 22], spectral measurements [23], multiphoton entangled states [24], and high-power continua in holey fibers [25].

A unique character of optomechanical nonlinearity is the generation of high-order sidebands, the field frequency components distanced exactly by the mechanical oscillation frequency, due to the energy transfer between the cavity field modes and the mechanical mode of a cavity optomechanical system (OMS) [17, 18, 26]. For practical applications

OMOFCs must have more sidebands. However, the comb lines of the previously achieved OMOFCs are rather limited, only around dozens or hundreds as reported by Refs. [17, 19, 20]. A much more improved setup combining thermal-optic effect can make 938 comb lines at a laser power of 448 mW [18]. For many applications such as precision optical metrology, such limited numbers of comb lines are not enough. A straightforward method for broadening comb span is to use higher pump power. However, the OMS can enter the regimes of chaos under very strong drive intensity, and the tremendously increased intracavity photons would damage the micro-cavity after turning on the strong pump laser for a period of time. An effective way to beat the bottleneck is crucial to the next stage of developing practical OMOFCs.

As we will see later, the frequency span of an OMOFC is determined by how large the associated mechanical oscillation amplitude can be realized. Therefore, the more energy is transferred to the mechanical resonator, the wider the output cavity field spectrum will be. Here, we propose an approach of efficiently adding up the mechanical energy based on a newly discovered resonance mechanism [26]: the mechanical oscillation of an unresolved-sideband OMS will be significantly enhanced under a two-tone driving field, with the difference of its tone frequencies being matched to the intrinsic mechanical frequency of the OMS. In this scenario the pump power for generating OMOFCs can be reduced to the level of only μW for obtaining dozens of comb lines. On the level of milliwatt (mW), more than 10000 comb lines can be generated with the currently available technologies. A system optimized further can realize the frequency combs with even broader spans.

Another important issue for frequency combs is their stability, i.e., to preserve the comb lines perfectly equidistant for a period as long as possible, for hours and even for days. In the past experiments optical spring effect is unavoidable, depending on the drive power and resulting in unpredictable me-

* bing.he@umayor.cl

† qlin@hqu.edu.cn

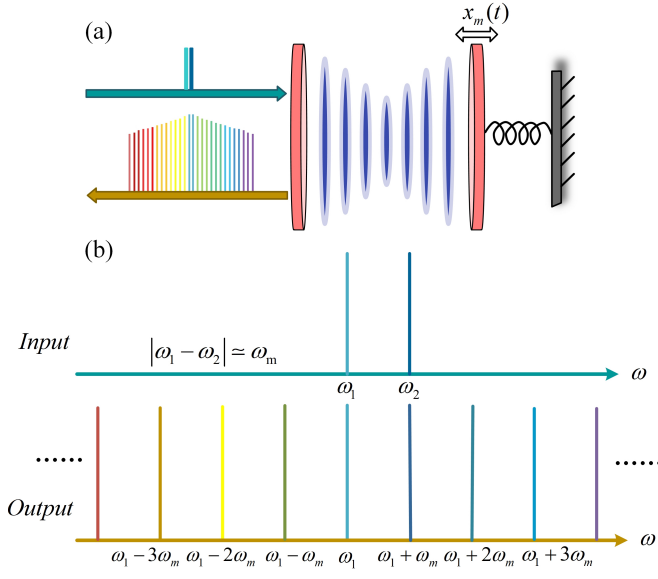


FIG. 1. Generic setup for generating optomechanical frequency combs. (a) A two-tone pump laser field drives the optical cavity with a movable mirror as the mechanical resonator. If the frequency difference $|\omega_1 - \omega_2|$ of the two tones gets close to the mechanical frequency ω_m , a special nonlinear resonance of optomechanics can be induced, leading to a significantly enhanced mechanical oscillation and the corresponding broadband cavity field as the frequency comb. (b) Typical spectrum of the driving field and the intracavity field with high-order sidebands generated by the consecutive interaction with the mechanical mode, which is quantitatively described by Eq. (1).

chanical frequency shift that changes the comb line distance. Our adopted nonlinear resonance also has a property of mechanical frequency locking, rendering the comb line distance be locked to be close to the intrinsic mechanical frequency of the system, totally independent of the applied drive power. It can thus practically guarantee the stability of the generated OMOFCs.

The rest of the paper is organized as follows. In Sec. II, the mechanism of realizing large mechanical oscillation by a special two-tone driving field is detailed in comparison with the corresponding mechanism due to a single-tone laser field, to illustrate the important features of broadband OMOFC and the associated oscillation frequency locking. The optimization of the concerned OMOFC by a parallel displacement of the drive tones is discussed in Sec. III. All factors affecting the performance of the system, including the drive intensity and intrinsic mechanical frequency are illustrated in Sec. IV. Then the technical requirements for the used drive tones is sketched in Sec. V, before the final part of conclusive remarks.

II. MECHANISM OF GENERATING BROADBAND OMOFC

The system we consider is a generic OMS, which is represented by the Fabry-Perot cavity in Fig. 1: the movable

mirror acts as a mechanical resonator with frequency ω_m and the cavity is pumped by a two-tone laser field with their frequencies ω_1 and ω_2 , respectively. The radiation pressure of the cavity field, which is proportional to the photon number $|a|^2 = (X_c^2 + P_c^2)/2$ (X_c and P_c are two quadratures of the field), drives the mechanical resonator into oscillation once the pump field satisfies a certain condition. As the first-order correction to the cavity field energy by the mechanical displacement under radiation pressure, there is the interaction potential

$$V_{int} = -g_m X_m |a|^2 \quad (1)$$

for the cavity field and mechanical resonator, where g_m is the optomechanical coupling strength at the single photon level. Here we have introduced the dimensionless mechanical displacement X_m by the scaling $x_m = \sqrt{\frac{\hbar}{m\omega_m}} X_m$ (m is the effective mass of the mechanical resonator), and the conjugate dimensionless momentum P_m is defined by another scaling $p_m = \sqrt{m\hbar\omega_m} P_m$. Then the dynamical equations of the system are given in the rotation frame with respect to the cavity frequency ω_c as follows:

$$\begin{aligned} \dot{a} &= -\kappa a + ig_m X_m a + \sum_{n=1,2} E_n e^{i\Delta_n t}, \\ \dot{X}_m &= \omega_m P_m, \\ \dot{P}_m &= -\omega_m X_m - \gamma_m P_m + g_m |a|^2 + \sqrt{2\gamma_m} \xi_m(t), \end{aligned} \quad (2)$$

where the detuning is defined as $\Delta_{1(2)} = \omega_c - \omega_{1(2)}$. The cavity damping rate κ includes the coupling rate to the external field κ_e and the intrinsic loss κ_i , so that $\kappa = \kappa_e + \kappa_i$. The drive amplitudes are determined by the pump power P as $E_{1(2)} = \sqrt{2\kappa_e P / \hbar\omega_{1(2)}}$. Moreover, at the room temperature, the thermal noise can be treated as a white noise satisfying the correlation $\langle \xi_m(t) \xi_m(t') \rangle = (2n_{th} + 1) \delta(t - t')$ [27], where $n_{th} = (e^{\hbar\omega_m/k_B T} - 1)^{-1}$ is the thermal phonon number at the temperature T . This thermal noise can be simulated with a stochastic function [28], but it does not have a significant effect on the concerned dynamical processes [26], so we will ignore it and adopt a mean-field approximation in the following discussions.

II.1. Field sidebands due to a single-tone drive

First, we take a look at the scenario when an OMS is driven by a single-tone pump field. When the power of the pump field is higher than a certain threshold of Hopf bifurcation, the system will enter the coupled oscillations of cavity field and mechanical resonator. The mechanical oscillation generally stabilizes in the form

$$X_m(t) = A_m \cos(\Omega_m t) + d_m, \quad (3)$$

where A_m denotes the oscillation amplitude and d_m a pure displacement with $d_m \ll A_m$. It should be noted that, due to the existence of optical spring effect, the frequency Ω_m can considerably differ from the intrinsic mechanical frequency

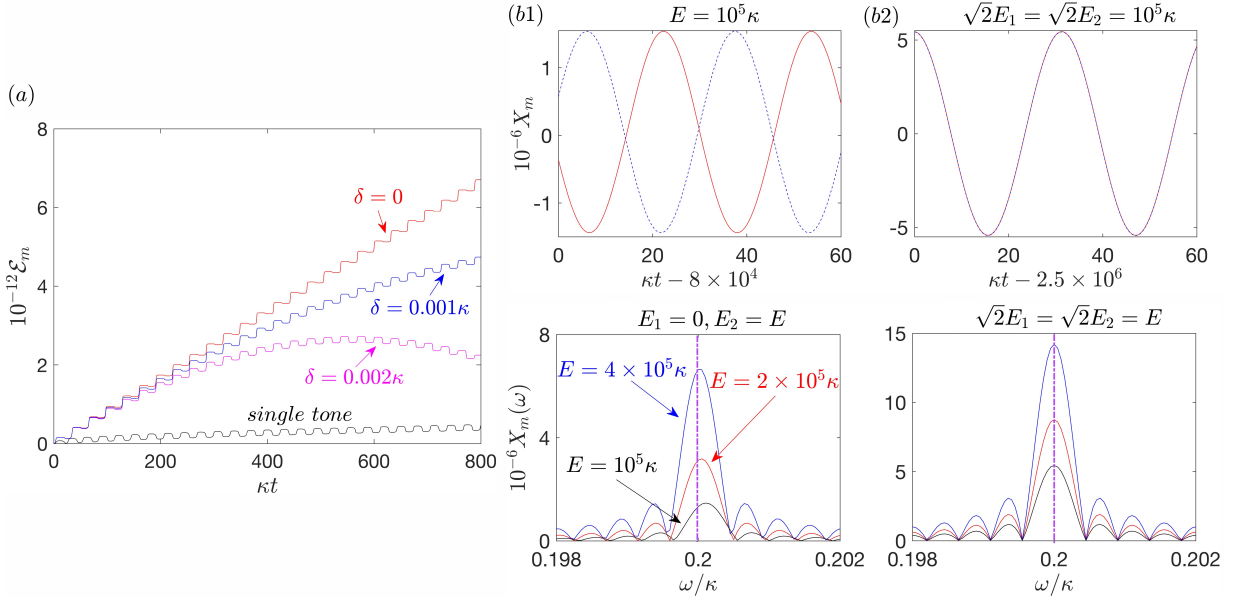


FIG. 2. A self-organized optomechanical resonance and its associated mechanical frequency locking. (a) The emergence of the resonance under the condition $\delta = 0$ in Eq. (6). The increased mechanical energy is at a rate much higher than the corresponding one under a single-tone pump of the same power. (b1)-(b2) The stabilized mechanical oscillation (the red solid curve) is compared with a reference oscillation at the frequency ω_m (the blue dashed curve)—the single-tone scenario shows their phase difference accumulated from a slight difference in their frequencies, but the two-tone scenario shows their exact overlap due to a frequency locking (the system has completely stabilized during the illustrated period of time, as the evolution time has been much larger than γ_m^{-1}). Moreover, the mechanical frequency shifts due to optical spring effect are obvious in the scenario of single-tone pump, in contrast to the completely locked mechanical frequency at the intrinsic one ω_m by the two-tone pump (the peaks of mechanical spectrum for all different drive amplitudes E are exactly at the point $\omega = \omega_m$). In the unresolved sideband regime where the stabilized cavity field is pulsed, a higher pump power gives rise to less spring effect for the system driven by a single-tone pump, because the cavity field pulse becomes narrower. The used parameters are $g_m = 10^{-5}\kappa$, $\omega_m = 0.2\kappa$, $\gamma_m = 10^{-5}\kappa$. In (a) the drive amplitude is $\sqrt{2}E = 10^5\kappa$.

ω_m , which is determined by the fabrication of the system. If one plugs this $X_m(t)$ into the first equation of Eq. (2), which is reduced to the situation of a single-tone drive, there will be the evolved cavity field in the form $a(t) = \sum_n a_n e^{in\Omega_m t}$ (up to a global phase), where

$$a_n = E \sum_p \frac{J_{n-p}(g_m A_m / \Omega_m) J_p(-g_m A_m / \Omega_m)}{ip\Omega_m + \kappa + i(g_m d_m - \Delta)}, \quad (4)$$

with $J_p(x)$ being the Bessel function of the first kind (see the derivation in Appendix). All these components $a_n = |a_n| e^{i\varphi_n}$ are called sidebands of the cavity field, from which it can be seen that their phases φ_n are fixed under a set of given system parameters, but the different sidebands have their different oscillation phases. The variable $g_m A_m / \omega_m$ of the Bessel functions is highly relevant to the sideband structure. There is one property of the Bessel function: given a fixed x , the magnitude of the p -th order Bessel function $J_p(x)$ will decay quickly if $|p| > |x|$; this property also guarantees the convergence of the summation in Eq. (4). Then, the value of $g_m A_m / \Omega_m$ determines to which sideband p the cavity field can have. In other words, the condition $p < g_m A_m / \Omega_m$ or $-p > -g_m A_m / \Omega_m$ specifies a range

$$-g_m A_m < \Delta\omega < g_m A_m \quad (5)$$

covering all possible sidebands with their frequency $p\Omega_m$ ($p \in \mathbb{Z}$) in a reference frame rotating at the pump laser frequency. The argument $g_m A_m / \Omega_m$ of the Bessel functions in Eq. (4) happens to be the half of the comb line number of the generated cavity field as frequency comb (the extension to the negative integers p gives the other half). Broad comb span should be certainly obtained by having a large mechanical amplitude A_m . The straightforward way for having a large A_m is to enhance the drive amplitude E , but the drive power cannot be increased without a limit because the accompanying heat would damage the systems. As reported by a recent experiment [18], a large pump detuning to the blue-detuned side can also increase the mechanical amplitude due to a peculiar system dynamics of OMS (see the discussions in Sec. 3). Another approach for having more sidebands is to make of the unresolved sideband regime ($\omega_m < \kappa$), where pulsed cavity field can be generated [29–31]. It is easy to reach the unresolved sideband regime by adjusting the pump-field coupling rate κ_e for a system with fixed intrinsic mechanical frequency ω_m . In what follows, we will consider this unresolved sideband regime for the designs of OMOFCs.

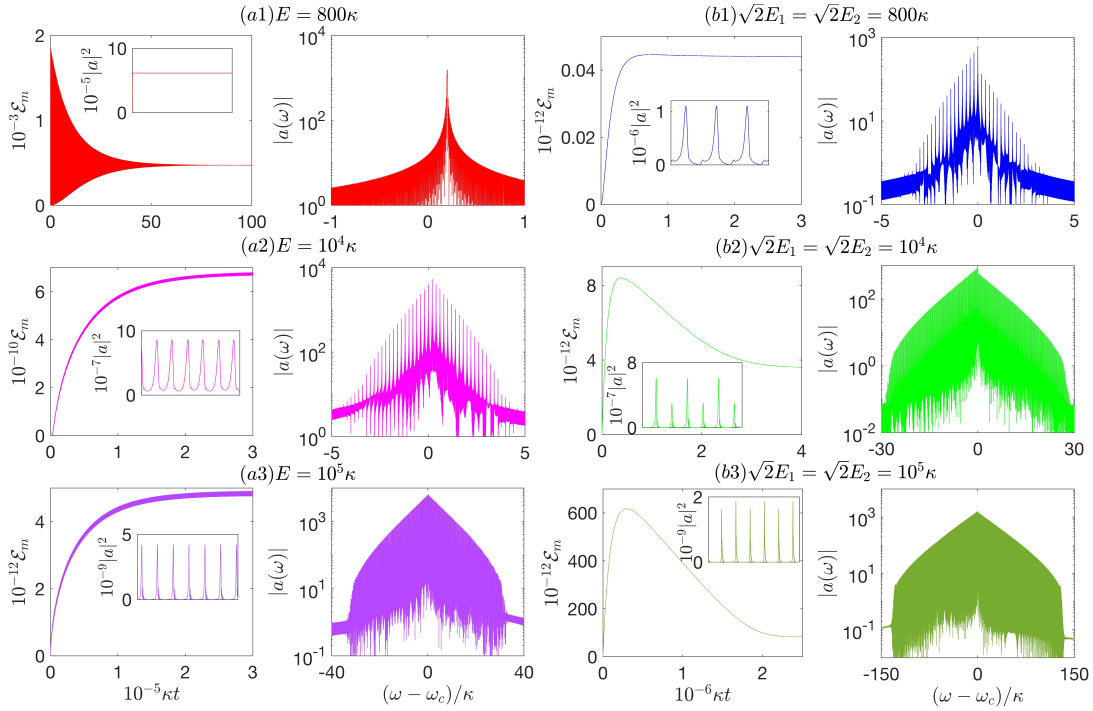


FIG. 3. Comparisons of the stabilized OMOFCs generated by a single-tone field at $\Delta = -\omega_m$ and a two-tone field with $\Delta_1 = -\omega_m$ and $\Delta_2 = 0$. Given the same pump power, the comb span of the latter is obviously much wider. The inset in each panel shows the stabilized cavity field intensity corresponding to the stabilized mechanical energy \mathcal{E}_m . As the pump amplitude E is increased, the illustrated field pulses become narrower, having a broader span of the generated OMOFC. The system parameters are chosen as $g_m = 10^{-5}\kappa$, $\omega_m = 0.2\kappa$, and $\gamma_m = 10^{-5}\kappa$.

II.2. Enhanced optomechanical oscillation by a special two-tone pump

The sideband amplitude in Eq. (4) is based on an already realized mechanical amplitude A_m , which is through a complicated dynamical process that must consider the coupled nonlinear equations Eq. (2). All similar processes vary with the applied pump field. If the single-tone pump is replaced by a two-tone driving field, the stabilized mechanical amplitude will have totally different patterns. The two tones with their corresponding detunings Δ_1 and Δ_2 satisfy the relation:

$$|\Delta_1 - \Delta_2| = \omega_m + \delta, \quad (6)$$

where the deviation δ can be any real number. Once the above difference between the two tones gets close to the intrinsic mechanical frequency ω_m , i.e. $\delta \rightarrow 0$, the system being operated in the unresolved sideband regime ($\omega_m < \kappa$) will exhibit a resonance phenomenon shown in Fig. 2(a). Generally, various nonlinear resonances can occur when a particular nonlinear oscillator has the maximum response to an external drive [32]. Our concerned resonance is out of a self-organization of the system when it is operated under the two conditions, $|\Delta_1 - \Delta_2| = \omega_m$ and $\omega_m/\kappa < 1$ [26]. In the unresolved sideband regime satisfying $\omega_m/\kappa < 1$, two cavity field pulses are generated in each mechanical oscillation period; one of them emerges when the mechanical resonator approaches its positive top speed in the oscillation period, but the other manifests

when it is close to its negative top speed (the radiation force of the pulse is opposite to the moving direction of the mechanical oscillator). Under a further condition $\delta = 0$, the field pulse acting in the opposite direction of the mechanical resonator's movement will be significantly suppressed, so the other pulse acting along with the movement of the mechanical resonator will successively add more and more energy

$$\mathcal{E}_m = \frac{1}{2}X_m^2 + \frac{1}{2}P_m^2 \approx \frac{1}{2}A_m^2 \quad (7)$$

to it, in the form of a quasi-linear energy increase in Fig. 2(a). Such tremendously increased mechanical amplitude A_m surely gives rise to a broadband $2g_m A_m$ of the cavity field, since, according to the reduced dynamics of the cavity field part [by plugging the stabilized mechanical oscillation $X_m(t)$ into the first equation of Eq. (2)], the stabilized mechanical amplitude A_m still determines the cavity field frequency span so that the range in Eq. (5) is valid (such sideband ranges can be accurately verified by the numerical calculations with our concerned two-tone drives). More features of the used nonlinear resonance are detailed in Ref. [26]. The main point of the current work is how to utilize this mechanism to realize good-quality OMOFCs.

In the resolved sideband regime $\omega_m \gg \kappa$, a two-tone field satisfying the condition $\delta = 0$ realizes a complete locking of an OMS: the mechanical oscillation amplitude, the mechanical oscillation frequency, as well as the oscillation phase, can be fixed without varying even after a considerable change of

the pump power and the associated noise effects, once the system has stabilized [33, 34]. These properties can be applied for various precise sensing [35–37]. The system operating in the unresolved sideband regime of $\omega_m/\kappa < 1$ also inherits the property of frequency locking. Due to the existence of optical spring effect, there is an unavoidable and mostly obvious shift of the actual mechanical oscillation frequency Ω_m from the intrinsic mechanical frequency ω_m determined by system fabrication, when the system is driven by a single-tone field. An intuitive view of the effect is that the difference between the two frequencies, Ω_m and ω_m , will accumulate a phase difference between the actual mechanical oscillation and a reference mechanical oscillation at the frequency ω_m , after the oscillations proceed for a period of time; see Fig. 2(b1). This effect causes a problem of instability of frequency combs’ repetition rates, as it was observed by the measurement of the Allan deviations with changed pump powers [18]. However, if the same single-tone pump field is split into two components with the difference of their frequencies matching the intrinsic mechanical frequency ω_m , the stabilized mechanical oscillation will well keep its frequency to the intrinsic one ω_m , as seen from the exactly coinciding actual and reference oscillation in Fig. 2(b2). It is even clearer to see the oscillation frequency locking by comparing the mechanical spectrum induced by the single-tone and double-tone pump, which are in the lower panel of Fig. 2(b1) and Fig. 2(b2), respectively. More generally, the mechanical oscillation frequency is locked to the frequency difference $|\Delta_1 - \Delta_2|$ of two drive tones, as long as the error δ in Eq. (6) is within a certain range. Such a frequency locking is independent of the applied pump power and totally robust against noise perturbations.

II.3. OMOFC broadened with an optomechanical resonance

The advantages of the two-tone pump satisfying $|\Delta_1 - \Delta_2| = \omega_m$ are clearer by a comparison with the corresponding single-tone pump; see Fig. 3. In the right part of Fig. 3, the corresponding pumps of a single tone (in the left part) are divided into two with one of them being shifted to a different frequency of $\Delta_2 = 0$. Dozens of comb lines can be obtained with a rather low pump power proportional to E^2 , while the system driven by a single-tone drive below its Hopf bifurcation point stabilizes to a static equilibrium; compare Figs. 3(a1) and 3(b1). The comb span in Fig. 2(b1) is close to that in Fig. 2(a2), where the pump power is, however, increased by 156 times. In Fig. 3(b3) the number of comb lines has been beyond 1000 and, given the experimental setup in Ref. [18], this OMOFC can be achieved with a pump power below 100 mW. Because we split an original pump into two tones, the corresponding comb teeth brightness will be lower due to the energy conservation. The brightness will be improved if both pump tones have the same power as in the corresponding single-tone scenario. For example, given the pump field of $E_1 = E_2 = 10^4\kappa$ for the process in Fig. 3(b2), the amplitude of the highest comb tooth will be increased to 5.21×10^3 , well close to the corresponding one with 5.28×10^3 in Fig. 3(a2).

Different patterns of adding up mechanical energy explain

the difference in the generated OMOFCs. As seen from Figs. 3(a2) and 3(a3), the mechanical energy \mathcal{E}_m under a single-tone pump increases in a manner of asymptotic stabilization with time. A stronger pump drives the same system to a higher mechanical energy, but the energy increase rate is not so significant. On the other hand, the system driven by a two-tone field satisfying $|\Delta_1 - \Delta_2| = \omega_m$ exhibits a rapid growth of mechanical energy due to a self-organized resonance at the beginning stage of time evolution [26]. Only after this stage, will the system gradually tend to a stabilization in a process dominated by its mechanical damping. The asymptotic behaviors of the systems operated in the unresolved sideband regime ($\omega_m < \kappa$) are very different from those in the resolved sideband regime ($\omega_m \gg \kappa$), where the optomechanical interaction enhances the mechanical damping so that the total effective damping rate is increased with an extra term Γ_{opt} [38]. Optomechanical cooling processes in the regime of resolved sideband are therefore much faster than the mechanical relaxation characterized by the time γ_m^{-1} [39–41]. In contrast, a cavity field realized in an unresolved sideband regime becomes pulsed, affecting the mechanical resonator only within a short period of time. Therefore, the intrinsic mechanical damping rate γ_m determines the stabilization in the regime of $\omega_m < \kappa$. From Fig. 3 one sees that the processes under a single-tone pump stabilize after a time in the order of γ_m^{-1} but, due to the existence of a nonlinear resonance, the dynamical processes under the concerned two-tone drives are modified and take even longer time than γ_m^{-1} when they become finally stabilized. An even clearer comparison between the single-tone scenario and our concerned two-tone scenario is displayed in Fig. 4, where the achieved mechanical amplitudes A_m under the lower drive amplitude E have the totally different tendencies—there is a definite Hopf bifurcation point to start optomechanical oscillation for the single-tone scenario (a behavior called “phonon laser” [38]), but the optomechanical oscillation induced by the concerned two-tone pump has a continuous existence towards $E = 0$ [26]. The realized bandwidths $2g_m A_m$ of OMOFCs by the concerned two-tone pump fields, therefore, significantly surpass those by the corresponding single-tone pump fields.

The adopted exemplary system in Figs. 3 and 4 has a mechanical quality factor $Q = 2 \times 10^4$. Due to the extremely slow stabilization processes caused by the optomechanical resonance, we have not simulated the dynamical evolution with a still smaller mechanical damping γ_m . OMOFCs covering much more sidebands are expected with the still improved mechanical quality factors. The continued discussions will be about how to achieve the better OMOFCs by the adjustment of other system parameters under the proper conditions.

III. OPTIMIZATION OF OMOFC SIMPLY BY DETUNING

Driven by a single-tone pump, there are two tendencies for a stabilized cavity field intensity, $|a(t)|^2 = \sum_n A_n \cos(n\Omega_m t + \phi_n)$ (ϕ_n is the phase for the n -th sideband), with the increased blue detuning of the pump. One is certainly that the overall cavity field will dwindle as the pump is off the resonance. But the other is an energy redistribution

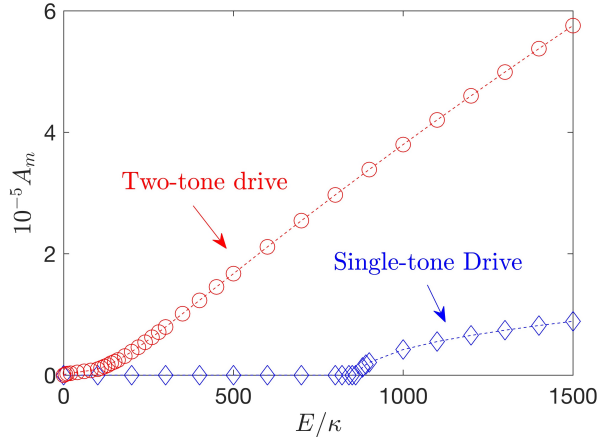


FIG. 4. Comparison of the realized mechanical oscillation amplitudes by a single-tone pump and a corresponding two-tone pump. In the two-tone scenario the optomechanical oscillation exists with tiny amplitude near $E = 0$. In the single-tone scenario, on the other hand, a Hopf bifurcation at $E \approx 880\kappa$ starts the oscillation from $A_m = 0$, and it is evidenced by a critical slowing-down near the point (in Fig. 3(a) the stabilization process close to the bifurcation has been rather slow). Here the system parameters are the same as those in Fig. 3.

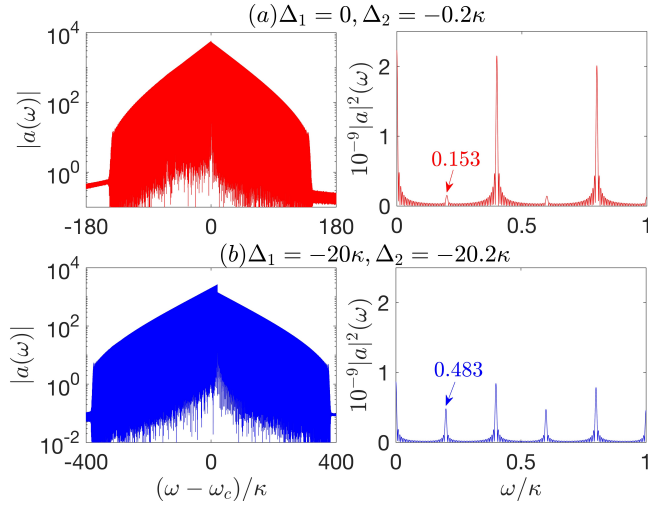


FIG. 5. Illustration of the effect by a parallel displacement of two tones. From (a) to (b), both tones are displaced to more blue-detuned side by an amount of 20κ , so that the comb span becomes broadened. The peak of the spectrum in (b) is shown to be shifted to $\omega = \omega_c + 20\kappa$, and the amplitudes of all sidebands less than this peak frequency are enhanced. One result of the process is that the indicated first sideband magnitude A_1 on the right side of (a) is increased to the one on the right side of (b). Here the drive amplitude is $\sqrt{2}E = 4 \times 10^5\kappa$, with all other parameters being the same as those in Fig. 3.

among the field sidebands so that the first sideband of $|a(t)|^2$ with its magnitude, $A_1 = 2|\sum_p \alpha_{p+1}\alpha_p^*|$, will be enhanced. This first sideband with the magnitude A_1 predominantly determines the mechanical amplitude A_m since it is the closest to the mechanical resonance frequency ω_m among all those with their magnitudes A_n , and an enhanced magnitude A_1 by

blue detuning will thus increase the bandwidth $2g_m A_m$ of the generated OMOFC. These two tendencies compete with each other in the determination of the sideband magnitude A_1 , and give rise to an optimum pump detuning for the bandwidth of OMOFC, beyond which the comb span will drop instead. An experimental demonstration of such enhancement by blue detuning is reported in Ref. [18], which shows the generation of the OMOFCs with about 1000 comb lines by a large detuning further increased by a thermal-optic effect.

When it comes to our concerned two-tone pump scenario, there is also a similar enhancement of comb span by varying drive tones. The previously mentioned optomechanical resonance still exists after the application the following displacements [26]:

$$\Delta_1 \rightarrow \Delta_1 + \delta\omega, \quad \Delta_2 \rightarrow \Delta_2 + \delta\omega, \quad (8)$$

for the two tones of the pump from their original frequencies of $\Delta_1 = 0$, $\Delta_2 = -\omega_m$ we have adopted before. All features of the applied optomechanical resonance are well preserved as long as the two tones satisfy the condition $|\Delta_1 - \Delta_2| = \omega_m$. Now we demonstrate that an appropriate displacement $\delta\omega_m$ to the blue-detuned side can considerably broaden the comb span, as shown in Fig. 5 where a displacement of $\delta\omega = -20\kappa$ extends the original comb span by about 2.64 times.

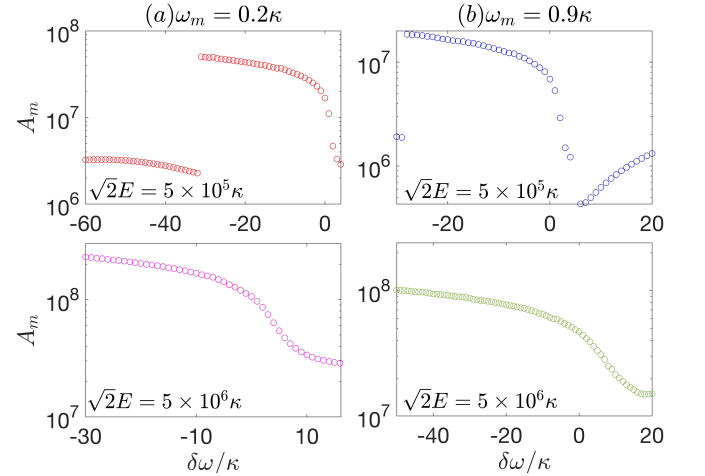


FIG. 6. Induced mechanical amplitude A_m under frequency displacement $\delta\omega$ of two drive tones for two different mechanical frequencies and two drive amplitudes. A suitable displacement can efficiently enhance the mechanical amplitude. In the two upper panels, the amplitude A_m reaches the maximum at $\delta\omega = -32\kappa$ for $\omega_m = 0.2\kappa$ and at $\delta\omega = -29\kappa$ for $\omega_m = 0.9\kappa$. Given a higher pump power as in the lower panels, the possible displacement range can be extended further to reach an optimum point, for example, $\delta\omega = -137\kappa$ for $\omega_m = 0.2\kappa$ and $\delta\omega = -116\kappa$ for $\omega_m = 0.9\kappa$ (the curves extending to the left sides will be broken and drop down at these points). The fixed parameters are the same as those in Fig. 3.

Such spectrum broadening of OMOFC by a parallel displacement of the drive tones can be understood with a slight asymmetry of the comb spectrum shown in Fig. 5(b). The parallel displacement will move the peak of the optical spectrum

from the original position at $\omega = \omega_c$ to a displaced position at $\omega = \omega_c + |\delta\omega|$, and the sidebands with their frequencies less than the original peak frequency will be enhanced after the displacement; see Fig. 5(b). This asymmetry amplifies the first sideband magnitude A_1 in the optical field intensity spectrum $|a|^2(\omega)$, as indicated by the values numerically obtained in Fig. 5. Like in a single-tone scenario [18], a larger mechanical amplitude A_m due to the enhanced sideband magnitude A_1 will therefore lead to a further extended comb span $2g_m A_m$.

In Fig. 6, we show the relations between the dimensionless mechanical amplitude A_m and the frequency displacement $\delta\omega$ for two different systems with their mechanical frequencies $\omega_m = 0.2\kappa$ and 0.9κ , which are also respectively driven by one two-tone pump of $\sqrt{2}E = 5 \times 10^5\kappa$ and another two-tone pump of $\sqrt{2}E = 5 \times 10^6\kappa$. The comb span can be broadened further by about three times for the lower drive power, while it can be broadened by about 2.2 times for the higher drive amplitude. For the system described in Fig. 3, the comb line number will be more than 10000 after the dimensionless mechanical amplitude is higher than $A_m = 10^8$. In the upper panels of Fig. 6, such improvement will be stopped at where the curve of A_m is broken at the blue detuning with $|\delta\omega| = 32\kappa$ for $\omega_m = 0.2\kappa$, as well as at $|\delta\omega| = 29\kappa$ for $\omega_m = 0.9\kappa$. These points indicate the optimum comb spans around there. The applicable displacement range can be increased further with a still larger drive amplitude E , as shown in the two lower panels of Fig. 6. Overall, the associated dynamical processes modified by drive-tone displacements are rather complicated due to the relevance of various factors.

IV. PERFORMANCE WITH VARIED PUMP POWERS AND DUE TO DIFFERENT SYSTEM FABRICATIONS

So far, we have discussed on the figures-of-merit of the OMOFC generated by a specified two-tone drive on an OMS, which is operated by adjusting the pump-cavity coupling κ_e to an unresolved sideband regime $\kappa > \omega_m$. In addition to locking the mechanical oscillation frequency to near the intrinsic one ω_m , the comb span can be enlarged by times if one simply displaces the tones together to a proper detuning. A more obvious factor is the pump power $P = \hbar\omega_{1(2)}E^2/(2\kappa_e)$. In Fig. 7(a) we illustrate how the realized mechanical amplitude A_m changes with the associated two-tone drive amplitude E . The realized amplitude A_m for the different ω_m increases linearly with the drive amplitude [note that a logarithmic scale is used for the vertical axis of Fig. 7(a)]. If the system fabrication can enhance the optomechanical coupling g_m to the level of $10^{-4}\kappa$, all systems with the used ω_m in Fig. 7(a) can realize the frequency comb line numbers $2g_m A_m/\omega_m > 10000$ under the low pump powers, which achieve the dimensionless mechanical amplitude A_m beyond 10^7 . Like the systems driven by a single-tone pump in unresolved sideband $\omega_m/\kappa < 1$ [17], those under a two-tone drive with the frequency difference $|\Delta_1 - \Delta_2|$ close to ω_m encounter less problem of chaos when the pump power is extremely high, so the room for applying strong pump is big as long as the systems

can withstand the heating by the intensified pulses in their cavities.

The mechanical frequency ratio ω_m/κ is another important factor to determine the comb span. Its relation with the realized mechanical amplitude is shown in Fig. 7(b). Especially, within the range of $\omega_m/\kappa < 0.1\kappa$, the mechanical amplitude increases rapidly with this decreased ratio. For example, at the ratio $\omega_m/\kappa = 0.05$, about 10500 comb lines can be obtained with a relatively low drive amplitude $E = 10^5\kappa$. More than 30500 comb lines can be realized under the same pump power if the ratio ω_m/κ is decreased further to 0.01.

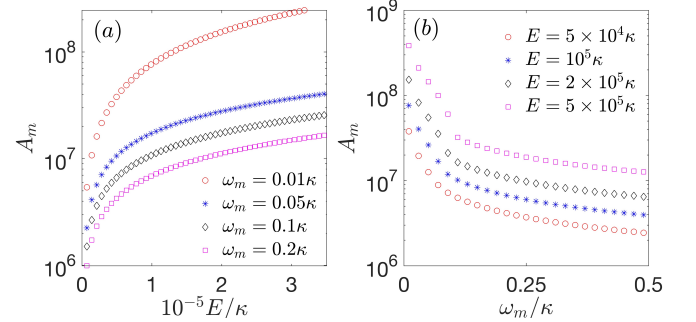


FIG. 7. Realizable mechanical oscillation amplitudes A_m due to varied drive amplitude (a) or different mechanical frequencies (b). A large mechanical amplitude is possible with a high pump power or a small mechanical frequency. The fixed system parameters adopted in these simulation are $g_m = 10^{-5}\kappa$, $\Delta_1 = 0$, $\Delta_2 = -\omega_m$, and $Q = \omega_m/\gamma_m = 1500$.

One method for a small ratio ω_m/κ is to have a higher rate κ_e for the coupling between the pump and the cavity. However, it will also affect the other system parameters, especially the optomechanical coupling ratio g_m/κ . Then, it is better to have a mechanical mode with lower intrinsic frequency ω_m , which can be realized by the fabrication to a different geometry of OMS. A smaller ω_m certainly implies a less spring restoring force proportional to $-\omega_m^2 X_m$ and thus a larger oscillation amplitude A_m . From the view of photon-phonon interaction, a cavity photon with its energy $\hbar\omega_c$ will absorb (release) more phonons with a less energy $\hbar\omega_m$, so that it can be converted to more of those with the frequencies $\omega_c + n\omega_m$ ($\omega_c - n\omega_m$), where n is an integer, to have a broader spectrum in Fig. 1(b). On the other hand, the cavity damping rate κ can be regarded as the line width of the cavity field. In a good regime of generating OMOFCs, one such line width encompasses a large quantity of the sidebands distanced by the mechanical frequency ω_m .

For example, given the experimentally achievable parameters $\omega_m = 0.05\kappa = 5\pi$ MHz and $Q = 1500$, together with an optomechanical coupling tuned to $g_m = 2.3 \times 10^{-5}\kappa$ by the total cavity field damping rate $\kappa = 2\pi \times 50$ MHz, 9500 comb lines can be obtained by the use of a two-tone pump with the detunings $\Delta_1 = 0$ and $\Delta_2 = -0.05\kappa$. The required pump power corresponding to the drive amplitude $\sqrt{2}E = 10^5\kappa$ is 32.1 mW for the pump laser of 1550 nm. Furthermore, the comb lines can be increased to 22500 by simply displacing the detunings to $\Delta_1 = -10\kappa$, $\Delta_2 = -10.05\kappa$. When the pump

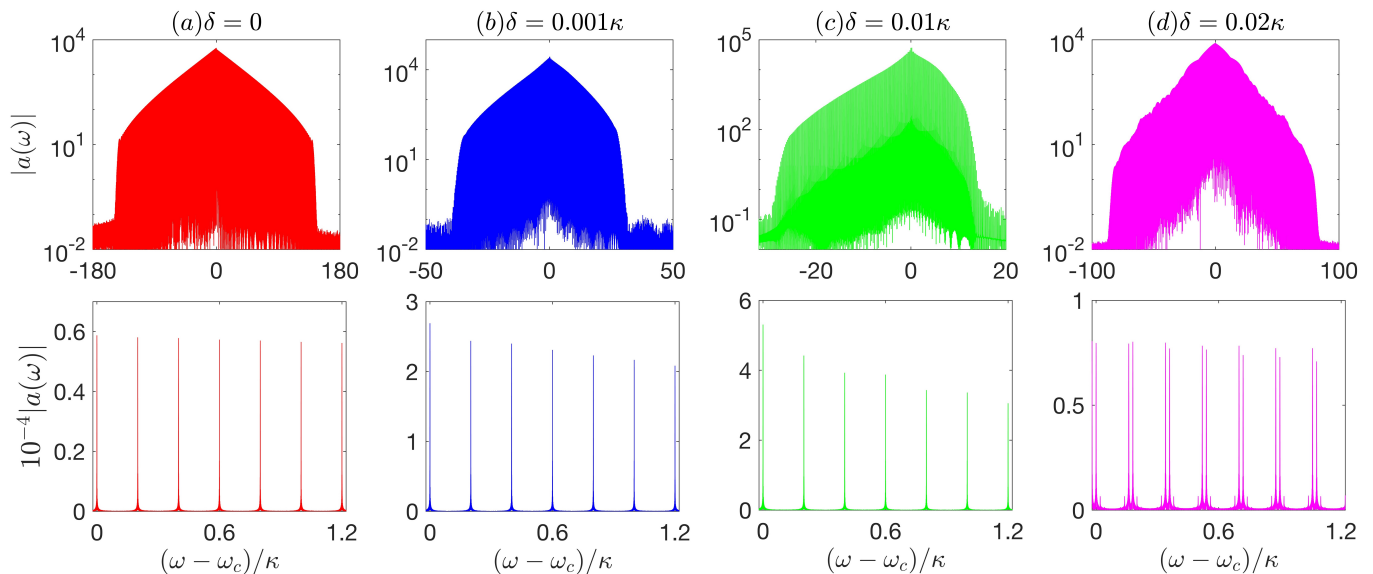


FIG. 8. Possible consequences of imperfect frequency tone matching. The comb span or bandwidth is seen to be reduced by a larger error δ in Eq. (6). From (a) to (c), the distance between the comb teeth is $\omega_m + \delta$. After the error becomes as large as $\delta = 0.02\kappa$, however, different sets of sidebands will be generated. These results are based on the system in Fig. 3 by fixing the drive amplitude of the two tones at $\sqrt{2}E = 4 \times 10^5 \kappa$.

power is decreased to 8.03 mW, there will be 11150 comb lines realized by the pump with the detunings $\Delta_1 = -6.0\kappa$ and $\Delta_2 = -6.05\kappa$. It should be noted that, for the convenience of reaching the final stability more quickly (see the discussion in Sec. 2.3), the mechanical quality factor Q used for our simulations is low, and the better OMOFCs are expected to realize with a slight improvement on the quality of mechanical resonator. An even better improvement is with the optomechanical coupling strength g_m . If it can be increased by one order, a much enlarged comb span $2g_m A_m$ can be realized with the pump powers reduced by two orders.

V. IMPERFECT DRIVE-TONE CONDITIONS

In realistic situations, there exists an unavoidable error δ in Eq. (6) for the two tones of the driving field. This error δ could come from the fluctuation of the frequencies of a pump laser. To have a clear view of how this error would affect the generated OMOFC, we illustrate the effects from various errors in Fig. 8, which is also based on the exemplary process in Fig. 3. From Fig. 8(a) to Fig. 8(b), one sees that the generated OMOFC will only lose some sidebands to a smaller span $2g_m A_m$, if the error δ is within $10^{-3}\kappa$. This defect can be compensated by a parallel displacement of the two tones as in Fig. 5(b). For a setup with $\kappa \sim 2\pi \times 10$ MHz, the requirement on $\delta \sim 10^{-4}\kappa$ specifies that the distance between two drive tones should not deviate from the frequency ω_m by more than $2\pi \times 1$ kHz. It is feasible to apply acoustic-optic modulator (AOM) [42] or single-sideband modulator (SSB) [43] to keep the error of two tones within the range. If a spectrum analysis of the mechanical oscillation is performed, one will see that the mechanical oscillation frequency under such a small error

$|\delta|$ will be locked to the difference $|\Delta_1 - \Delta_2|$ of the two drive tones. Up to the error $\delta = 10^{-2}\kappa$ in Fig. 8(c), the mechanical oscillation frequency, as well as the distance between the individual sidebands, is still locked to the difference $|\Delta_1 - \Delta_2|$, totally independent of the applied pump power. Therefore, the stability of the generated OMOFCs relies on how good we can control the frequency fluctuations of two drive tones.

However, given a still larger error up to $\delta = 2 \times 10^{-2}\kappa$ for the exemplary system in Fig. 8, the dynamics of the system will become totally different. The effect of self-organized resonance will be lost, but the system never behaves as if it were under two independent drives. In this situation the two drive tones will realize other cooperative effects. First of all, more mechanical frequency components, such as the fractional ones, will emerge while the peak of the mechanical spectrum $X_m(\omega)$ returns to the original mechanical frequency ω_m from $|\Delta_1 - \Delta_2|$. The corresponding cavity field sidebands will therefore split into a number of different sets; the two main sets will be shifted to the frequency positions $\Delta_1 + n\omega_m$ and $\Delta_2 + n\omega_m$ (n are integers), respectively, as shown in Fig. 8(d). By a further variation of the error δ , the system will enter chaos or other complicated quasi-periodic oscillations. The dynamical patterns in the regimes of unmatched pump tones with $\delta \neq 0$ are determined by the ratio ω_m/δ ; see more details in Ref. [26].

VI. CONCLUSION

The comb span of OMOFCs generated by an OMS is simply proportional to the mechanical oscillation amplitude it can possibly realize. We have investigated an effective approach to add up the mechanical energy of oscillation for the OMS,

so that it can realize broadband OMOFCs under feasible conditions. It is to operate the OMS in the regime of unresolved sideband and pump it by a two-tone field with the frequency difference of the drive tones being close to its intrinsic mechanical frequency. Then the system will be in a nonlinear resonance that quickly enlarges the mechanical oscillation amplitude and, purely through the intrinsic mechanical damping, it will stabilize to a final mechanical oscillation of significantly enhanced amplitude. Such enhanced mechanical oscillation amplitude can be increased further simply by choosing the proper detunings of the drive tones. A better operation point in the parameter space of the system will continually improve the generated OMOFC. With the experimentally feasible setups based on the mechanism, frequency comb lines of more than 10^4 can be realized under pump powers in the order of mW. A very useful feature of the mentioned nonlinear resonance is that the mechanical oscillation frequency can be well locked to the frequency difference of the two drive tones. The resulting OMOFC pulse repetition rate and comb teeth spacing can be thus locked without any change by the pump power. It is therefore possible to achieve a good stability of the generated OMOFC by controlling the frequency fluctuations of two drive tones. The currently illustrated scenario, which is implementable by a specified two-tone pump, may reduce the distance to the real applications of OMOFCs.

APPENDIX

Here we provide a derivation of the exact sideband amplitudes for the evolved cavity field $a(t)$ under a single-tone drive. After substituting the stabilized mechanical oscillation in Eq. (3) in to the first equation of Eq. (2), which has been reduced to the situation of a single-tone drive, we obtain the

following effective equation about the cavity field:

$$\dot{a} = -\kappa a + ig_m A_m \cos(\Omega_m t) a + ig_m d_m a + E e^{i\Delta t}. \quad (\text{A-1})$$

By a transformation $a(t) = e^{i\Delta t} e^{ig_m A_m \sin(\Omega_m t)/\Omega_m} a_1(t)$, the above equation will be reduced to

$$\dot{a}_1 = -\kappa a_1 - i\Delta a_1 + ig_m d_m a_1 + E e^{-ig_m A_m \sin(\Omega_m t)/\Omega_m}. \quad (\text{A-2})$$

Then, we make use of the generating function of the Bessel functions, $e^{(z/2)(x-1/x)} = \sum_{n=-\infty}^{\infty} J_n(z)x^n$, where $z = -gA_m/\Omega_m$ and $x = e^{i\Omega_m t}$, in the drive term of Eq. (A-2) and solve it as a linear differential equation. The solution is

$$a_1(t) = \sum_{n=-\infty}^{\infty} E \frac{J_n(-g_m A_m / \Omega_m)}{in\Omega_m + \kappa + i(g_m d_m - \Delta)} e^{in\Omega_m t}. \quad (\text{A-3})$$

Using the generating function of the Bessel functions again, we obtain

$$a(t) = \sum_{l=-\infty}^{\infty} \sum_{n=-\infty}^{\infty} E \frac{J_l(g_m A_m / \Omega_m) J_n(-g_m A_m / \Omega_m)}{in\Omega_m + \kappa + i(g_m d_m - \Delta)} \times e^{i\Delta t + (l+n)\Omega_m t}, \quad (\text{A-4})$$

the coefficients of which can be combined to the form in Eq. (4).

ACKNOWLEDGMENTS

This work was supported by National Natural Science Foundation of China (Grant No. 12374348), and ANID Fondecyt Regular (1221250). The authors thank Dr. Ming Li for helpful discussions.

-
- [1] S. A. Diddams, Th. Udem, J. C. Bergquist, *et al.*, "An optical clock based on a single trapped $^{199}\text{Hg}^+$ ion," *Science* **293**, 825-828 (2001).
- [2] M. T. Murphy, Th. Udem, R. Holzwarth, *et al.*, "High-precision wavelength calibration of astronomical spectrographs with laser frequency combs," *Mon. Not. R. Astron. Soc.* **380**, 839-847 (2007).
- [3] F. R. Giorgetta, W. C. Swann, L. C. Sinclair, *et al.*, "Optical two-way time and frequency transfer over free space," *Nat. Photon.* **7**, 434-438 (2013).
- [4] C. Gohle, Th. Udem, M. Herrmann, *et al.*, "A frequency comb in the extreme ultraviolet," *Nature* **436**, 234-237 (2005).
- [5] R. J. Jones, K. D. Moll, M. J. Thorpe, *et al.*, "Phase-coherent frequency combs in the vacuum ultraviolet via high-harmonic generation inside a femtosecond enhancement cavity," *Phys. Rev. Lett.* **94**, 193201 (2005).
- [6] F. Keilmann, C. Gohle, and R. Holzwarth, "Time-domain mid-infrared frequency-comb spectrometer," *Opt. Lett.* **29**, 1542-1544 (2004).
- [7] I. Coddington, W. C. Swann, L. Nenadovic, *et al.*, "Rapid and precise absolute distance measurements at long range," *Nat. Photon.* **3**, 351-356 (2009).
- [8] J. Pfeifle, V. Brasch, M. Lauerer, *et al.*, "Coherent terabit communications with microresonator Kerr frequency combs," *Nat. Photonics* **8**, 375-380 (2014).
- [9] D. J. Jones, S. A. Diddams, J. K. Ranka, *et al.*, "Carrier-envelope phase control of femtosecond mode-locked lasers and direct optical frequency synthesis," *Science* **288**, 635-639 (2000).
- [10] R. Holzwarth, T. Udem, T.W. Hänsch, *et al.*, "Optical Frequency Synthesizer for Precision Spectroscopy," *Phys. Rev. Lett.* **85**, 2264-2267 (2000).
- [11] A. Parriaux, K. Hammani, and G. Millot, "Electro-optic frequency combs," *Adv. Opt. Photonics* **12**, 223-287 (2020).
- [12] P. Del'Haye, A. Schliesser, O. Arcizet, *et al.*, "Optical frequency comb generation from a monolithic microresonator," *Nature*, **450**, 1214-1217 (2007).

- [13] T. J. Kippenberg, R. Holzwarth, and S. A. Diddams, "Microresonator-based optical frequency combs," *Science* **332**, 555-559 (2011).
- [14] T. J. Kippenberg, A. L. Gaeta, M. Lipson, *et al.*, "Dissipative Kerr solitons in optical microresonators," *Science* **361**, eaan8083 (2018).
- [15] A. L. Gaeta, M. Lipson, and T. J. Kippenberg, "Photonicchip-based frequency combs," *Nat. Photonics* **13**, 158-169 (2019).
- [16] J. C. Shi, Q. X. Ji, Q. T. Cao, *et al.*, "Vibrational kerr solitons in an optomechanical microresonator," *Phys. Rev. Lett.* **128**, 073901 (2022).
- [17] M.-A. Miri, G. D'Aguanno, and A. Alù, "Optomechanical frequency combs," *New J. Phys.* **20**, 043013 (2018).
- [18] Y. Hu, S. L. Ding, Y. C. Qin, *et al.*, "Generation of optical frequency comb via giant optomechanical oscillation," *Phys. Rev. Lett.* **127**, 134301 (2021).
- [19] R. C. Ng, P. Nizet, D. Navarro-Urrios, *et al.*, "Intermodulation of optical frequency combs in a multimode optomechanical system", *Phys. Rev. Research* **5**, L032028 (2023).
- [20] G.-T. Xu, M. Zhang, Y. Wang, *et al.*, "Magnonic Frequency Comb in the Magnomechanical Resonator," *Phys. Rev. Lett.* **131**, 243601 (2023).
- [21] N. Picqué and T.W. Hänsch, "Frequency comb spectroscopy," *Nat. Photonics* **13**, 146-157 (2019).
- [22] N. Wilson, N. B. Hébert, C. Perrella, *et al.*, "Simultaneous observation of nonlinear magneto-optical rotation in the temporal and spectral domains with an electro-optic frequency comb," *Phys. Rev. Applied* **10**, 034012 (2018).
- [23] Y. Bao, X. Yi, Z. Li, *et al.*, "A digitally generated ultrafine optical frequency comb for spectral measurements with 0.01-pm resolution and 0.7- μ s response time," *Light Sci. Appl.* **4**, e300 (2015).
- [24] C. Reimer, M. Kues, P. Roztocky, *et al.*, "Generation of multiphoton entangled quantum states by means of integrated frequency combs," *Science* **351**, 1176-1180 (2016).
- [25] P. A. Champert, S. V. Popov, and J. R. Taylor, "Generation of multiwatt, broadband continua in holey fibers," *Opt. Lett.* **27**, 122-124 (2002).
- [26] Q. Lin, Y. Wu, G. Li, *et al.*, "Nonlinear optomechanical resonance entering a self-organized energy transfer pattern," *Chaos Soliton. Fract.*, **173**, 113624 (2023); arXiv:2306.00282.
- [27] Q. Lin, B. He, and M. Xiao, "Entangling Two Macroscopic Mechanical Resonators at High Temperature," *Phys. Rev. Applied* **13**, 034030 (2020).
- [28] Q. Lin, B. He, and M. Xiao, "Catastrophic transition between dynamical patterns in a phonon," *Phys. Rev. Research* **3**, L032018 (2021).
- [29] M. Poot, K. Y. Fong, M. Bagheri, *et al.*, "Backaction limits on self-sustained optomechanical oscillations," *Phys. Rev. A* **86**, 053826 (2012).
- [30] M. Gao, F.-C. Lei, C.-G. Du, *et al.*, "Self-sustained oscillation and dynamical multistability of optomechanical systems in the extremely-large-amplitude regime," *Phys. Rev. A* **91**, 013833 (2015).
- [31] X. Xu, H. Pi, W. Yu, *et al.*, "On-chip optical pulse train generation through the optomechanical oscillation," *Opt. Express*, **29**, 38781-38795 (2021).
- [32] S. Rajasekar and M. A. Sanjuan, "Nonlinear resonances," Springer (2016).
- [33] B. He, Q. Lin, M. Orszag, *et al.*, "Mechanical oscillations frozen on discrete levels by two optical driving fields," *Phys. Rev. A* **102**, 011503(R) (2020).
- [34] Y. Wu, G. Li, B. He, *et al.*, "Amplitude and phase locking of mechanical oscillation driven by radiation pressure," *Phys. Rev. A* **105**, 013521 (2022).
- [35] G. Li, Y. Wu, Y. L. Zhang, *et al.*, "Ultra-high resolution mass sensing based on an optomechanical nonlinearity," *Opt. Express* **30**, 15858-15876 (2022).
- [36] Z.-F. Yan, B. He, and Q. Lin, "Force sensing with an optomechanical system at room temperature," *Phys. Rev. A* **107**, 013529 (2023).
- [37] Z.-F. Yan, B. He, and Q. Lin, "Optomechanical force sensor operating over wide detection range," *Opt. Express* **31**, 16535-16548 (2023).
- [38] M. Aspelmeyer, T. J. Kippenberg, and F. Marquardt, "Cavity optomechanics," *Rev. Mod. Phys.* **86**, 1391-1452 (2014).
- [39] B. He, L. Yang, Q. Lin, *et al.*, "Radiation pressure cooling as a quantum dynamical process," *Phys. Rev. Lett.* **118**, 233604 (2017).
- [40] C. Wang, Q. Lin, and B. He, "Breaking the optomechanical cooling limit by two drive fields on a membrane-in-the-middle system," *Phys. Rev. A* **99**, 023829 (2020).
- [41] B. He and Q. Lin, "Dynamical approach to quantum optomechanics: Motivation, method, and applications," *Fundamental Research* **3**, 87-89 (2023).
- [42] P. Verlot, A. Tavernarakis, T. Briant, *et al.*, "Backaction amplification and quantum limits in optomechanical measurements," *Phys. Rev. Lett.* **104**, 133602 (2010).
- [43] Z. Shen, Y.-L. Zhang, C.-L. Zou, *et al.*, "Dissipatively controlled optomechanical interaction via cascaded photon-phonon coupling," *Phys. Rev. A* **126**, 163604 (2021).